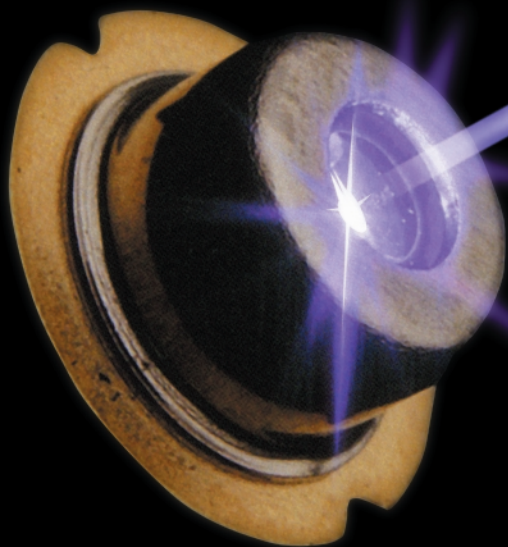


CURRENT STATUS AND FUTURE PROSPECTS OF InGaN-BASED LASER DIODES

Shuji NAKAMURA

UV InGaN and GaN single-quantum well structure light-emitting diodes (LEDs) were grown on epitaxially laterally overgrown GaN (ELOG) and sapphire substrates. When the emission wavelength of UV InGaN LEDs was shorter than 380 nm, the external quantum efficiency (EQE) of the LED on ELOG was much higher than that on sapphire, but only for high-current operation. At low-current operation, both LEDs had the same EQE. When the active layer was GaN, the EQE of the LED on sapphire was much lower than that on ELOG even for low- and high-current operations due to the lack of localized energy states formed by fluctuations in indium composition. In order to improve the lifetime of the laser diodes (LD), ELOG had to be used because the operating current density of the LD is much higher than that of the LED. A violet InGaN multi-quantum-well/GaN/AlGaIn separate confinement-heterostructure LD was grown on ELOG on sapphire. The LDs with cleaved mirror facets showed an output power as high as 40 mW under room-temperature continuous-wave (CW) operation. The stable fundamental transverse mode was observed at an output power of up to 40 mW. The estimated lifetimes of the LDs at a constant output power of 10 mW and 30 mW were more than 2,000 and 500 hours respectively, during CW operation at an ambient temperature of 60°C.



1. Introduction

The brightness and durability of light-emitting diodes (LEDs) makes them ideal for displays, while semiconductor laser diodes (LDs) have been used as a light source in applications ranging from optical communications systems to compact disk players. These applications have been limited, however, by a lack of materials that can emit blue light efficiently. Full-color displays, for example, require at least three primary colors, usually red, green and blue, if they are to produce every visible color. Such a combination is also needed to make a white-light emitting device that would be more durable and consume less power than conventional incandescent bulbs or fluorescent lamps. A shorter wavelength means that the light can be focused more sharply, which in turn increases the storage capacity of magnetic and optical disks. Digital versatile disks (DVDs), which came onto the market in 1996, rely on red AlInGaP semiconduc-

Department of Research and Development,
Nichia Chemical Industries, Ltd.,
491 Oka, Kaminaka, Anan, Tokushima 774, Japan
E-mail: shuji@nichia.co.jp

tor lasers and have a data capacity of about 4.7 gigabytes (Gbytes), compared to 0.65 Gbytes for compact disks (CDs) which use infrared lasers. By moving to violet wavelengths using III-V nitride-based semiconductors, the capacity could be increased to more than 15 Gbytes. The violet III-V nitride-based LDs could also improve the performance of laser displays, printers and undersea optical communications. III-V nitride-based semiconductors have a direct band gap that is suitable for blue light-emitting devices: the band gap energy of aluminum gallium indium nitride (AlGaInN) varies between 6.2 and 2.0 eV, depending on its composition, at room temperature (RT). Thus, by using these semiconductors, red to ultraviolet-emitting devices can be fabricated.

The first breakthrough for III-V nitride-based semiconductors was the use of AlN^{1,2)} or GaN^{3,4)} nucleation layers for the GaN growth. Using these nucleation layers it became possible to obtain high-quality GaN films with a mirror-like flat surface, a low residual carrier concentration, a high mobility and a strong photoluminescence (PL) intensity in spite of a large lattice mismatch of 15% between GaN and the sapphire substrate. The second big breakthrough for III-V nitride-based LEDs and LDs was not only that p-type GaN was obtained but that the reason why it had not been obtained before was also clarified.

For the LEDs and LDs, a p-n junction is used to inject holes and electrons into the active layers from the p-type layer and the n-type layer, respectively. Thus, both p-type and n-type conductivity control is necessitated to fabricate these devices. It was easy to obtain n-type GaN from the beginning. However, it was impossible to obtain p-type GaN films for a long time.^{5,6)} Unavailability of p-type GaN films had prevented the realization of light emitting diodes from III-V nitrides, such as blue LEDs and LDs. Since the 1970s, many people had tried to make p-type GaN by doping with, for ex-

ample Zn,⁷⁾ Be,⁸⁾ Mg,⁹⁾ and Cd¹⁰⁾ into GaN as an acceptor impurity.

However, the reason why a low-resistivity p-type GaN could not be obtained when GaN was doped with impurities was not clear. In 1989, Amano *et al.*¹¹⁾ obtained p-type GaN films using Mg-doping as an acceptor impurity followed by a post low-energy electron-beam irradiation (LEEBI) treatment using a metalorganic chemical vapor deposition (MOCVD) growth method. After the growth, LEEBI treatment was performed for Mg-doped GaN films to obtain a low-resistivity p-type GaN film. The effect of the LEEBI treatment was considered to be Mg displacement due to the energy of the electron beam irradiation. No one except Amano *et al.* had succeeded in obtaining p-type GaN until 1992 because the mechanism of the LEEBI treatment was not understood exactly.

In 1992, Nakamura *et al.*^{12,13)} obtained p-type GaN films using nitrogen post-ambient thermal annealing for Mg-doped GaN instead of the LEEBI treatment. Before thermal annealing, the resistivity of Mg-doped GaN films was approximately $1 \times 10^6 \Omega\text{cm}$. After thermal annealing at temperatures above 700°C the resistivity became $2 \Omega\text{cm}$.¹²⁾ Low-resistivity p-type GaN films, which were obtained by N₂-ambient thermal annealing, showed a resistivity as high as $1 \times 10^6 \Omega\text{cm}$ after NH₃ ambient thermal annealing at temperatures above 600°C.¹³⁾ They then proposed that atomic hydrogen produced by NH₃ dissociation at temperatures above 400°C was related to the acceptor compensation mechanism.¹³⁾ A hydrogenation process whereby acceptor-H neutral complexes were formed in p-type GaN films was proposed¹³⁾: the formation of acceptor-H neutral complexes causes acceptor compensation. This hydrogenation process has now been accepted as the acceptor compensation mechanism of p-type III-V nitride-based semiconductor by many researchers.¹⁴⁻¹⁸⁾ Theoretical calculations of this hy-

drogen passivation were undertaken by Neugebauer and Van de Walle.¹⁸⁾ Thus, in 1992, the 20-year mystery of p-type GaN was resolved.

The third big breakthrough was that high quality InGaN film became available. As mentioned above, the InGaN active layer is used for all of the III-V nitride based LEDs and LDs to emit red to uv light. Thus, InGaN is a very important compound semiconductor among III-V nitride compounds because the InGaN active layer emits light by the recombination of the injected electrons and holes into the InGaN. In spite of its importance, nobody had succeeded in obtaining high-quality InGaN films which could emit a strong band-to-band emission at RT by optical pumping or current injection.¹⁹⁻²¹⁾

In 1992, Nakamura and Mukai succeeded in growing high quality InGaN films for the first time, films which emitted a strong band to band emission from uv to green, by changing the In content of the InGaN using a novel two-flow MOCVD method.²²⁾ Finally, Nakamura *et al.*²³⁾ grew an InGaN multiple quantum well (MQW) structure and confirmed an enhanced strong PL intensity from the quantized energy levels of the InGaN well layer with a thickness of 25 μm. The addition of a small amount of indium into the GaN was very important in obtaining a strong band to band emission because GaN without the indium could not emit a strong band to band emission at RT. This reason is considered to be related to deep localized energy states.²⁴⁻²⁸⁾

Using the above-mentioned major breakthrough techniques, in 1994 Nakamura *et al.* developed the first blue InGaN/AlGaIn double heterostructure LEDs²⁹⁾ and then developed blue/green InGaN quantum well (QW) structure LEDs in 1995.³⁰⁾ Then, ultraviolet (UV)/amber LEDs^{31,32)} and the first demonstration of RT violet laser light emissions in InGaN/GaN/AlGaIn-based heterostructures under pulsed op-

eration were achieved.³³⁾ Since Nakamura *et al.* report of pulsed operation, many groups have reported pulsed operation of LDs using the same structure.³⁴⁻⁴⁰⁾ Then, the latest results showed that the lifetime became as long as 1,000⁴¹⁾ and 10,000 hours⁴²⁾ under RT continuous-wave (CW) operation. Also, high power LDs were fabricated using epitaxially lateral overgrown GaN (ELOG)⁴³⁾ and GaN substrates.⁴⁴⁾ Then, at last, Nakamura *et al.*⁴⁵⁾ succeeded in making the first commercially available products from violet InGaN-based LDs in February 1999.

All of these light-emitting devices use an InGaN active layer instead of a GaN active layer; because it is difficult to fabricate a highly efficient light-emitting device using a GaN active layer, the reason for this is still not well known. Also, the InGaN active layer in these LEDs and LDs includes a large number of threading dislocations (TDs) from 1×10^8 to 1×10^{12} cm⁻² originating from the interface between GaN and the sapphire substrate due to a large lattice mismatch of 15%.^{46,24)} The TDs are considered to be formed as a result of a complex set of interactions including the interface energy, the nucleation density, and island coalescence.⁴⁷⁾ In spite of these large numbers of dislocations, the efficiency of the InGaN-based LEDs and LDs is much higher than that of the conventional III-V compound semiconductor (AlGaAs and AlInGaP)-based LEDs and LDs. In many conventional optoelectronic devices, the device performance has been limited by the control of both point defects and structural defects in these materials. However, the most recent reports suggest that III-V nitride-based devices are less sensitive to dislocations than conventional III-V semiconductors.

Numerous studies have investigated the origin of these defects,⁴⁷⁾ and their effects on the structural,^{49,50)} optical,^{51,52)} electronic,^{53,54)} and morphological properties^{47,55-57)} of heteroepitaxial GaN layers. Rosner *et al.*⁵²⁾ char-

acterized the correlation between TDs as observed by transmission electron microscopy (TEM), surface morphology as observed by atomic force microscopy (AFM) and wavelength-resolved cathodoluminescence (CL) imaging. The dark areas in the CL images were regions of the film where minority carriers were depleted due to the high nonradiative recombination velocity at these dislocations. Sugahara *et al.*⁵⁸⁾ observed the TD at the same location in n-type GaN films using plan-view TEM and CL images to study the TDs. There was a clear one-to-one correspondence between the dark spots observed in the CL images and the dislocations in TEM images, indicating that the dislocations are nonradiative recombination centers. The minority carrier (hole) diffusion length was estimated to be approximately 50 nm by the analysis of the CL dark spots. Chichibu *et al.*⁵⁹⁾ studied the emission mechanisms of GaN and InGaN quantum wells (QWs) by comparing their optical properties as a function of TD density, which was controlled by a lateral epitaxial overgrowth (LEO) technique. PL intensity was slightly strengthened by reducing TD density from 1×10^{10} cm⁻² to nearly zero (less than 1×10^6 cm⁻²). Also, the major PL decay time was independent of the TD density.

These results suggested that the emission mechanisms are unaffected by TDs. TDs are considered to simply reduce the net volume of light-emitting area. The effect is less pronounced in InGaN QWs, where carriers are effectively localized at a certain potential minimum caused by In composition fluctuations in the QWs to form quantized excitons,²⁴⁻²⁸⁾ before being trapped in nonradiative pathways at TDs, resulting in a pronounced slow decay time (1-40 ns). The depth of these localized energy states with a small In composition fluctuation is enhanced by the large band gap bowing of the InGaN.⁶⁰⁾ Assuming that the lateral spacing of the effective bandgap (potential) minimum determines the carrier diffusion

length in InGaN, the carrier diffusion length was estimated to be less than 60 nm.²⁸⁾ Absence of change in the Stokes-like shift due to reduction of TD density revealed that the effective bandgap fluctuation in InGaN QWs was not due to a phase separation initiated by TDs.^{61, 62)}

Epitaxially laterally overgrown GaN (ELOG) on sapphire was developed recently to reduce the number of TDs in GaN epitaxial layers.^{44,63,64)} Using the ELOG, the number of TDs was reduced significantly in the GaN grown on a SiO₂ stripe mask. The blue InGaN single-quantum-well (SQW) structure LEDs were fabricated on the ELOG to study the role of dislocations.⁶⁵⁾ The output power of blue LEDs grown on the ELOG was almost the same as that grown directly on sapphire substrates at a forward current from 0 to 60 mA in spite of a large difference of TD density between both LEDs.¹³⁾ To explain the high efficiency and long lifetime of InGaN-based LEDs grown on sapphire, the existence of localized energy states formed by In composition fluctuations of InGaN layer was proposed.²⁴⁻²⁸⁾ For InGaN-based LDs, however, the TD density had to be decreased to lengthen the lifetime by using the ELOG. For InGaN-based LEDs, the lifetime of the LEDs is more than 100,000 hours in spite of the large number of dislocations.

This difference in lifetime-behavior between LDs and LEDs is probably caused by the difference in the operating current density in the two devices. The operating current density of LDs is about one order higher than that of LEDs. In order to study the role of dislocations in InGaN and GaN layers further, UV InGaN and GaN SQW-structure LEDs were fabricated on ELOG and sapphire substrates. We call these, UV InGaN and GaN SQW-structure LEDs, UV InGaN and GaN LEDs respectively, for simplicity. The performance of current InGaN-based LDs is also described here.

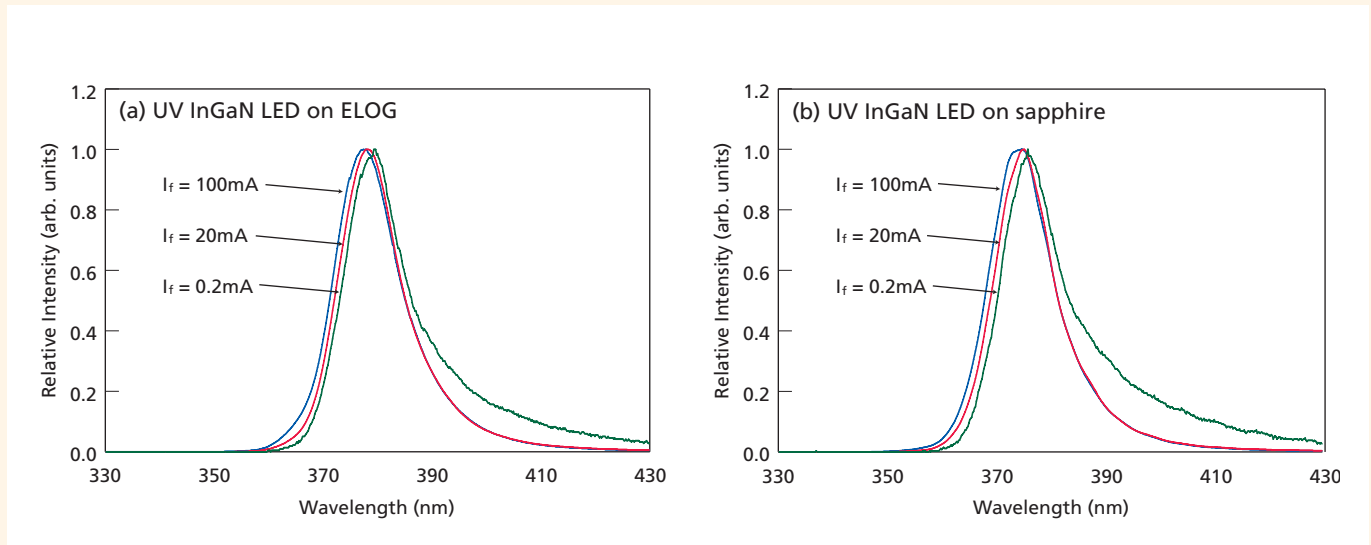


Fig. 1
 Emission spectra of UV InGaN LEDs on (a) ELOG and (b) sapphire substrates at various forward currents at RT.

2. UV InGaN and GaN LEDs grown on ELOG

III-V nitride films were grown using the two-flow metal-organic chemical vapor deposition (MOCVD) method, the details of which have been described previously.^{3,4} First, selectively grown on a 2 μm -thick GaN layer grown on a (0001) C-face sapphire substrate. The 0.1 μm -thick silicon dioxide (SiO_2) mask was patterned to form 4 μm -wide stripe windows with a periodicity of 12 μm in the GaN $\langle 1\bar{1}00 \rangle$ direction. Following the 15 μm -thick GaN growth on the SiO_2 mask pattern, the coalescence of the selectively grown GaN allowed the formation of a flat GaN surface over the entire substrate. The coalesced GaN was designated the ELOG.^{44,63,64}

We examined the defect density by plan-view transmission electron microscopy (TEM) observation of the surface of ELOG substrates. The number of dislocations on the SiO_2 mask area was close to zero and that on the window area was approximately $2 \times 10^7/\text{cm}^2$.⁴⁴ This ELOG was the same as that used to fabricate blue SQW LEDs previously.⁶⁵ After obtaining a 15 μm -thick ELOG substrate, UV InGaN and GaN LEDs were grown on the substrate.^{31,66} The growth conditions of each layer are de-

scribed elsewhere.³ The LED structure consists of a 1.5 μm -thick undoped GaN layer, a 2.4 μm -thick n-type GaN:Si layer, a 0.2 μm -thick undoped GaN layer (current spreading layer), a 400 \AA -thick n-type AlGaIn:Si, a 50 \AA -thick undoped InGaIn or GaIn active layer, a 600 \AA -thick p-type Al_{0.2}Ga_{0.8}N:Mg layer and a 0.1 μm -thick p-type GaN:Mg layer. The structure of these LEDs is almost the same as that of previous UV InGaIn LEDs.^{31,66} The In composition of the InGaIn well layer was close to zero for UV LEDs.^{31,66}

For comparison, LEDs of the same structure of LEDs were grown directly on sapphire substrate. The fabrication of LED chips (350 μm x 350 μm) was accomplished as follows: the surface of the p-type GaN layer was partially etched until the n-type GaN layer was exposed; next, a Ni/Au contact was evaporated onto the p-type GaN layer and a Ti/Al contact on to the n-type GaN layer. The characteristics of the LEDs were measured under a direct current (DC) at room temperature.

Figure 1 shows the emission spectra of UV InGaIn LEDs on ELOG and sapphire substrates at various currents at RT. The peak wavelength of both LEDs is around 380 nm. The large spectrum width is due mainly to fluctua-

tions in indium composition in the InGaIn well-layer.²⁴⁻²⁸ This means that the degree of fluctuations is the same in both LEDs in spite of a large difference in the TD density. Thus, the In composition fluctuations are not related to the TDs. In both spectra, a small blue-shift is observed due to the band-filling effect of the localized energy states formed by In composition fluctuations.²⁴⁻²⁸ However, the degree of blue-shift is relatively small due to the small In composition fluctuations that resulted from the small In composition in the InGaIn well-layer. The ELOG and GaIn on sapphire had average dislocation densities of $7 \times 10^6/\text{cm}^2$ and $1 \times 10^{10}/\text{cm}^2$ respectively. Here, the average dislocation density of the ELOG on sapphire was obtained by dividing the dislocation density of $2 \times 10^7/\text{cm}^2$ on the window region by the ratio of (stripe periodicity of 12 μm) / (window width of 4 μm) because the dislocation density on the SiO_2 stripe region was almost zero. The size of the LED chip is as large as 350 μm x 350 μm . Each LED chip includes many window and SiO_2 stripe regions. Therefore, we used an average dislocation density for the ELOG on sapphire.

Figure 2 shows the external quantum efficiency (EQE) of UV InGaIn and GaIn LEDs as a function of forward current. From this figure,

the EQE of UV InGaN LED on sapphire is almost the same as that on ELOG at low currents below 0.4 mA. Thus, the carriers are easily captured by localized energy states formed by In composition fluctuations at low currents, and radiatively recombine before they are captured by nonradiative recombination centers formed by a large number of dislocations.⁶⁷⁾ With increasing current, some carriers can overflow from the localized energy states due to a small In composition fluctuation of UV InGaN LEDs, and reach nonradiative recombination centers. As a result, the efficiency of UV InGaN LEDs on sapphire decreases at high currents. By reducing the dislocation density using ELOG, UV InGaN LEDs can emit a stronger power output even at high currents. On the other hand, the EQE of UV GaN LED on sapphire is lower than that on ELOG even at low currents because there are no localized energy states formed by In composition fluctuations. It is only by reducing the dislocation density, that the EQE of UV GaN LEDs can be increased using ELOG, as shown in Fig. 2.⁶⁷⁾

Recently, many groups have reported that the quantum-confined Stark effect (QCSE) resulting from the piezoelectric field due to strain determines the emission mechanism of InGaN or GaN-based LEDs.⁶⁸⁻⁷¹⁾ This field, if sufficiently strong, will induce a spatial separation of the electron and hole wave functions in the well. Then, the wave function overlap decreases and the inter-band recombination rate is reduced. It is difficult to explain the results in Fig. 2, by QCSE⁶⁷⁾: that is to say, the difference in the behaviour of UV InGaN and GaN LEDs, using UV InGaN LEDs on sapphire and ELOG have the same efficiency at low currents. However, the efficiency of UV GaN LED on sapphire is much lower than that on ELOG even at low currents. Considering the strain in the well-layer, QCSE should be almost the same for all of these LEDs. The results can be explained only by the localized energy states formed by In composition fluctuations as mentioned above, and not by QCSE.

Figure 3 shows EQE as a function of the emission wavelength of UV/blue/green InGaN LEDs with different In compositions. EQE is

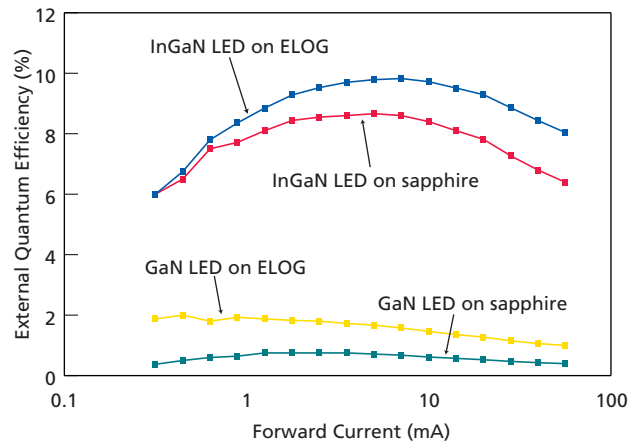


Fig. 2 EQE of UV InGaN and GaN LEDs as a function of forward current.

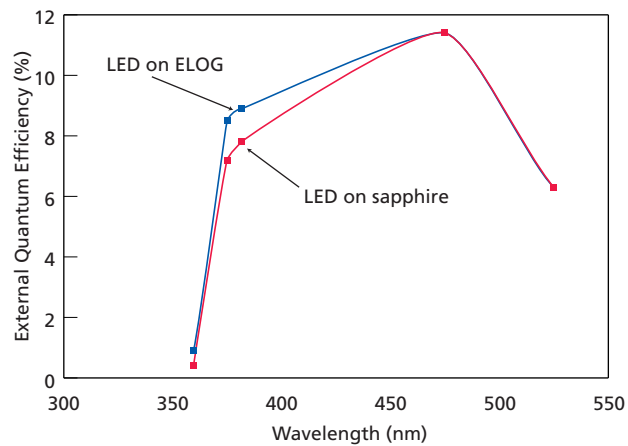
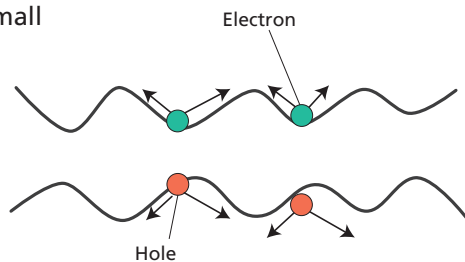


Fig. 3 EQE as a function of emission wavelength of UV/blue/green InGaN LEDs with different In compositions.

In composition fluctuation of $\text{In}_x\text{Ga}_{1-x}\text{N}$

1) X is small



2) X is large

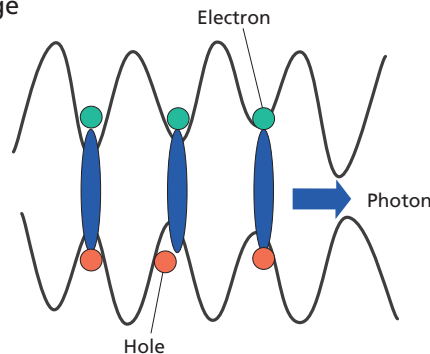


Fig. 4 Model of localized energy states formed by In composition fluctuations. (a) When the degree of In composition fluctuations is small, carriers easily overflow the localized states with increasing current. (a) When the degree of In composition fluctuations is large, carriers are still confined even at high current operation.

highest at a wavelength in the blue region due to a large number of deep localized energy states formed by large fluctuations in indium composition. At wavelengths in the blue and green regions, there was no difference in EQE between LEDs on ELOG and sapphire despite a large difference in the dislocation density between them.⁶⁵⁾ However, UV LEDs with an emission wavelength shorter than 380 nm exhibit a different behavior: EQE becomes much lower when the LED was fabricated on sapphire due to a large number of dislocations. When the emission wavelength of UV LEDs with an active layer of GaN is 360 nm, the EQE of GaN LEDs on ELOG is two times higher than that on

sapphire. These results can be explained by only using the localized energy states formed by In composition fluctuations in the InGaN well-layer, as mentioned in respect of Fig. 2. When electrons and holes are injected into the InGaN active layer of the LEDs, they are captured by the localized energy states before they are captured by the nonradiative recombination centers caused by a large number of threading dislocations. At these large localized energy states, localized excitons with a relatively high binding energy due to a quantum-well structure are formed for radiative recombination. When the In composition of the InGaN active layer is small, such as for UV LEDs, the In composition fluctu-

tuations become much smaller.

When electrons and holes are injected into this InGaN well-layer with a small In composition fluctuation, some of the injected carriers overflow from the localized energy states with increasing current and reach nonradiative recombination centers formed by a large number of dislocations. Then, the EQE becomes lower with increasing current, as shown in Figs. 2 and 3. Without In in the active layer, which means the GaN active layer, there are no In composition fluctuations to cause the formation of the localized energy states in the InGaN active layer. In this case, EQE is small even at low currents. However, EQE increases dramatically by reducing the number of dislocations using ELOG, as shown in Figs. 2 and 3, because the number of nonradiative recombination centers is decreased by reducing the number of dislocation densities. When the emission wavelength is shorter than 370 nm, EQE decreases dramatically, due mainly to the self-absorption of p- and n-GaN contact layers.

Taking QCSE into consideration in Fig. 3, it is difficult to explain why EQE gradually decreases with decreasing emission wavelength of InGaN LEDs from 470 nm to 370 nm in spite of decreasing the strain in the InGaN well-layer. These results can be explained only by the localized energy states formed by In composition fluctuations. The In composition of the InGaN well-layer decreases with decreasing emission wavelength of LEDs. This means that the degree of In composition fluctuation becomes much smaller with decreasing emission wavelength of LEDs. Then, some of the carriers injected into the InGaN well layer can overflow from the localized energy states due to a small number of shallow localized energy states, and then reach nonradiative recombination centers formed by a large number of dislocations, as shown in Fig. 4.

Figure 4 shows the schematic model of localized energy states formed by In composition fluctuations in the InGaN well layer. Thus, EQE becomes smaller when the emission wave-

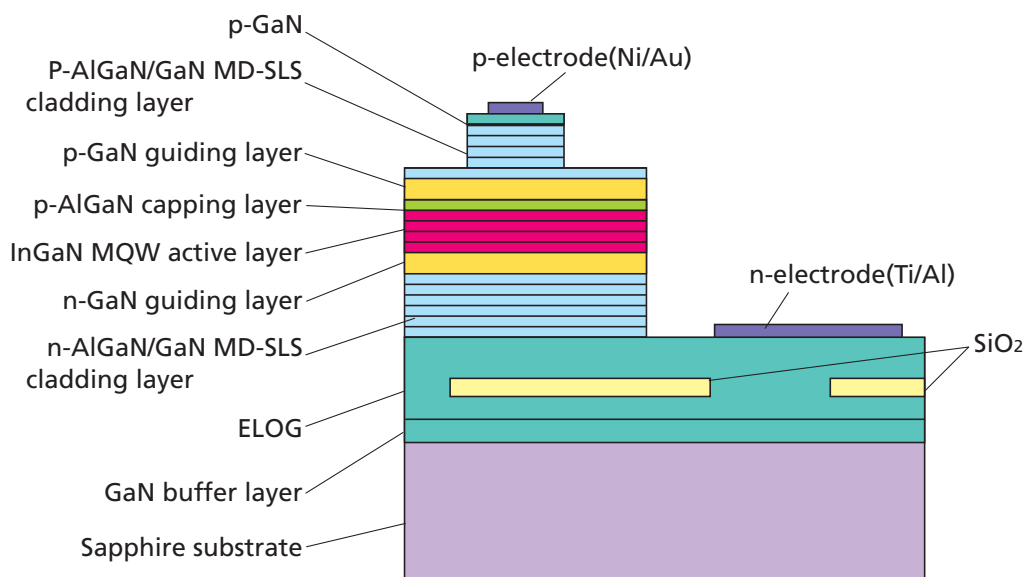


Fig. 5
Structure of InGaN-MQW/GaN/AlGaIn SCH laser diodes.

length becomes shorter. When the emission wavelength exceeds the blue region, EQE also decreases, as shown in Fig. 3, due to the poor crystal quality of the InGaIn layer: it is difficult to grow an InGaIn layer with a high In-content due to the phase separation of InGaIn during growth.⁷²⁾

3. Violet InGaIn-MQW/GaN/AlGaIn SCH LDs

Even if InGaIn active layers are used for LEDs and LDs, with increasing current, some carriers can overflow from the localized energy states due to a small In composition fluctuation of UV InGaIn LEDs and LDs, and reach

nonradiative recombination centers, as mentioned above. As a result, the efficiency of UV InGaIn LEDs and LDs on sapphire decreases at high current operation. The operating current density of the LDs (2-5 kA/cm²) is much higher (more than 10 times) higher than that of LEDs (0.04 kA/cm²). Thus, under laser operation, many carriers can overflow from the localized energy states, and reach nonradiative recombination centers formed by a large number of TDs when the LDs were fabricated directly on sapphire substrate.⁶⁷⁾ Through this nonradiative recombination of the carriers, the internal loss of the cavity of the LDs is increased, and the threshold current density of the LDs is increased.

⁶⁷⁾ As a result, the lifetime of the LDs was shortened to around 300 hours.^{73,74)} Thus, only by reducing the dislocation density using ELOG, can the lifetime of InGaIn-based LDs be lengthened by reducing the threshold currents.⁶⁷⁾ Here, the present performance of InGaIn-MQW/GaN/AlGaIn SCH LDs grown on ELOG is described.

On the above-mentioned ELOG substrate, the laser structure was grown as shown in Fig. 5. The details of the InGaIn-MQW/GaN/AlGaIn SCH laser structure are described in other papers.^{3,41-45)} The surface of the p-type GaIn layer was partially etched until the n-type GaIn layer and p-type Al_{0.15}Ga_{0.85}N/GaN MD-SLS cladding

layer were exposed to form the ridge-geometry LDs. The stripe width was 2 μm and the cavity length was 600 μm . The region of the ridge-geometry LD of 2 μm x 600 μm was formed on the laterally overgrown region of the GaN on SiO_2 stripe-shaped mask. A laser cavity was formed by cleaving the facets along the $\{1\bar{1}00\}$ face of the LD grown on the ELOG. A facet coating consisting of two pairs of quarter-wave $\text{TiO}_2/\text{SiO}_2$ dielectric multilayers was formed on one side of the facets. The output power of the LD was measured from an uncoated facet. The electrical characteristics of the LDs fabricated in this way were measured under a direct current (DC).

Figure 6 shows the voltage-current (V-I) characteristics and the light output power per uncoated cleaved facet of the LD as a function

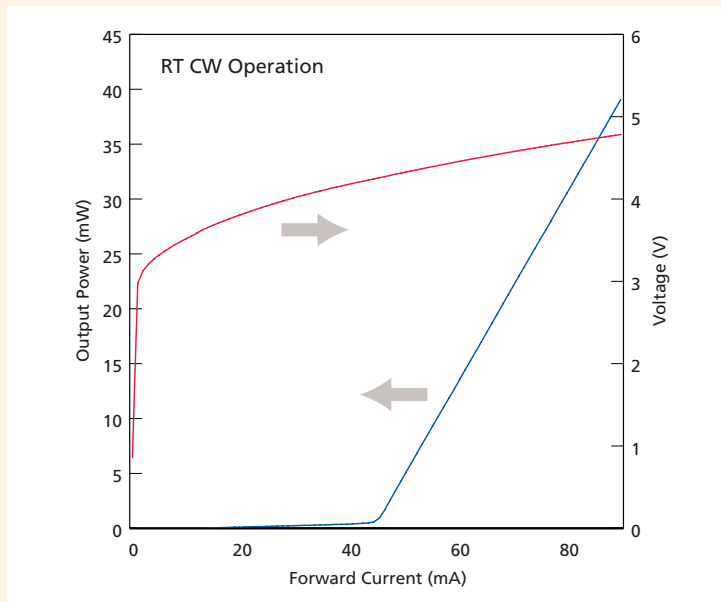


Fig. 6. Typical L-I and V-I characteristics of InGaN-MQW/GaN/AlGaIn SCH LDs measured under CW operation at RT.

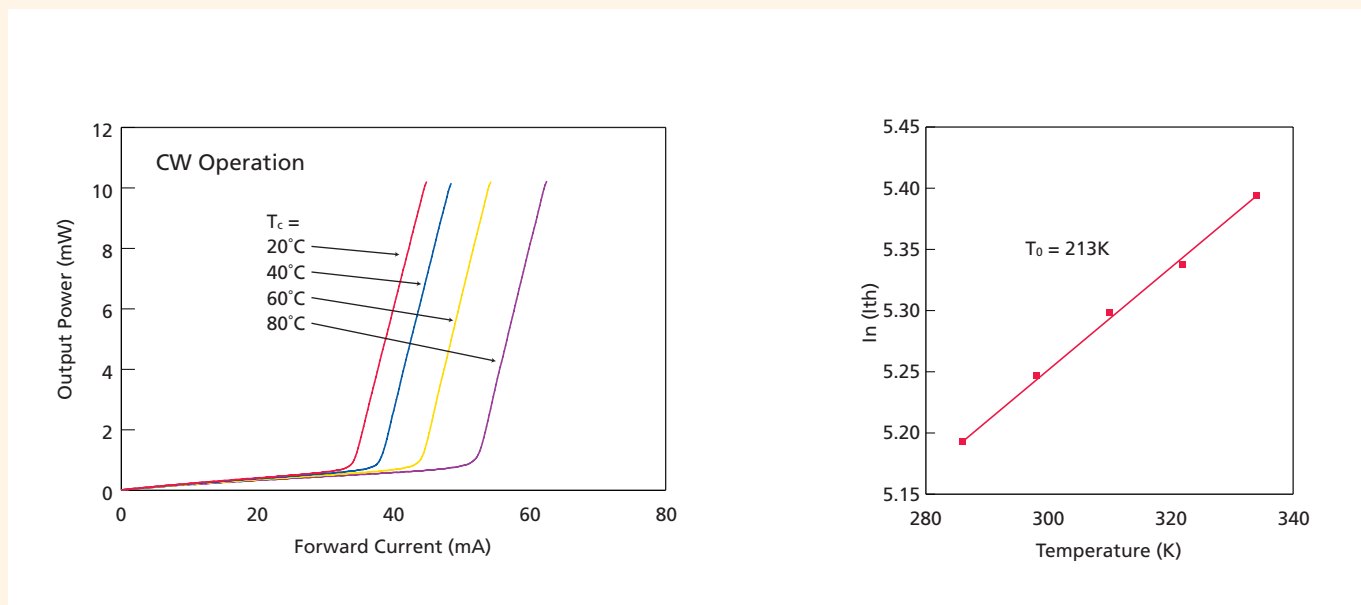


Fig. 7. L-I curves of InGaN-MQW/GaN/AlGaIn SCH LDs at various ambient temperatures.

Fig. 8. Threshold current of $I_{th}(T)$ as a function of the ambient temperature.

of the forward DC current (L-I) at RT. No stimulated emission was observed up to a threshold current of 43 mA, which corresponds to a threshold current density of 3.6 kA/cm². The threshold voltage was 4.3 V. The output power of the LDs was as high as 40 mW at an operating current of 90 mA. At an output power of up to 40 mW, no kink was observed in the L-I curve because the transverse mode was stable at a fundamental transverse mode with a small ridge width of 2 μm.⁷⁵⁾ The slope efficiency was as high as 1.0 W/A.

The temperature dependence of the L-I curves of the LDs was measured under CW operation at temperatures between 20°C and 80°C, as shown in Fig.7. The threshold current increased gradually with increasing temperature. The characteristic temperature T₀, which was used to express the temperature dependence of the threshold current in the form $I_{th}(T) = I_0 \exp(T/T_0)$, was estimated to be 213 K as shown in Fig. 8. Figure 8 shows the $\ln(I_{th}(T))$ as a function of temperature. Here, I₀ is a constant, T is the absolute temperature and I_{th}(T) is the threshold current. The value of this characteristic temperature was the highest one ever obtained in our group. The typical value of the characteristic temperature was around 150 K.

The measurement of the far-field patterns (FFPs) was performed, as shown in Fig. 9. At an output power of 30 mW, the FFP in the direction parallel (X) to the epitaxial layers collapsed to 9.7°; and the FFP extended to 24.9° in the perpendicular direction (Y). The aspect ratio was 2.6. This value is relatively small and is desirable for practical applications to condense a laser beam to a small spot size efficiently using collecting lens.

Next, the emission spectra of the LDs were measured under RT-CW operation, as shown in Fig.10. An optical spectrum analyzer (ADVANTEST Q8347), which utilizes a Fourier transform spectrometer with a Michelson interferometer, was used to measure the spectra

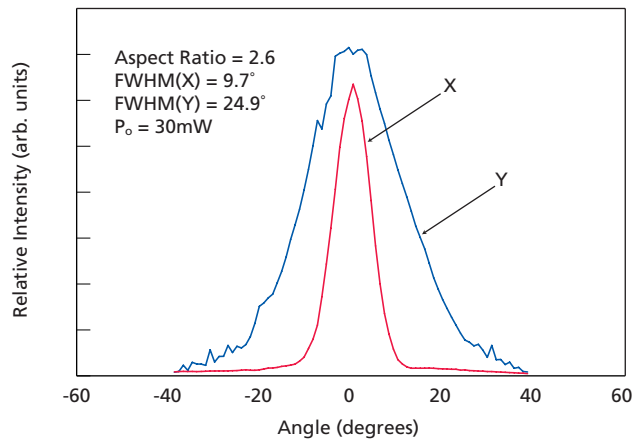


Fig. 9. FFP of InGaN-MQW/GaN/AlGaIn SCH LDs in the planes parallel (X) and perpendicular (Y) to the junction at an output power of 30 mW under RT-CW operation.

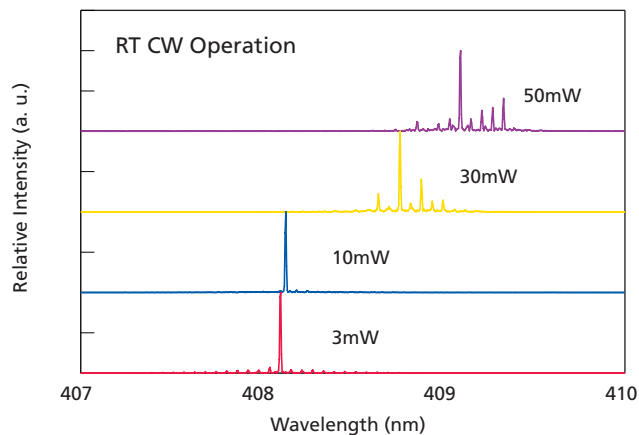


Fig. 10. Laser emission spectra measured under RT-CW operation at output powers of 3 mW, 10 mW, 30 mW and 50 mW.

of the LDs with a resolution of 0.001 nm. At output powers of 3 mW and 10 mW, single-mode laser emissions were observed at wavelengths of 408.1 nm and 408.2 nm. At output powers of 30 mW and 50 mW, multimode laser emissions were observed at wavelengths of 408.7 nm and 409.1 nm. Figure 11 shows the temperature dependence of the peak emission wavelength of three LDs under CW operation at an output power of 5 mW. During this measurement, the LDs were placed on a Peltier-type cooler to maintain the temperatures of the LDs between 10°C and 70°C. The average wavelength drift caused by the temperature change was estimated from this figure to be 0.06nm/K.

Figure 12 shows the results of a lifetime test of CW-operated LDs carried out at an ambient temperature of 60°C, in which the operating current is shown as a function of time under a constant output power of 10 mW controlled using an autpower controller (APC). After 78 hours of operation, only small degradation was observed. The degradation speed was defined to be dI/dt (mA/40 hours), where I is the operating current of the LDs and t is the time. Using this degradation speed, the estimated lifetime was determined to be the time when the operating current became 1.5 times the initial operating current of the LDs. The lifetime was estimated to be more than 2,000 hours under these conditions. For the application of writing DVDs and hard disk drives (HDDs), a high power of 30 mW is required. Figure 13 shows the results of a lifetime test of CW-operated LDs carried out at an ambient temperature of 60°C under a constant output power of 30 mW. In this case, the lifetime was estimated to be approximately 500 hours under the high-power of 30 mW and high-ambient-temperature of 60°C.

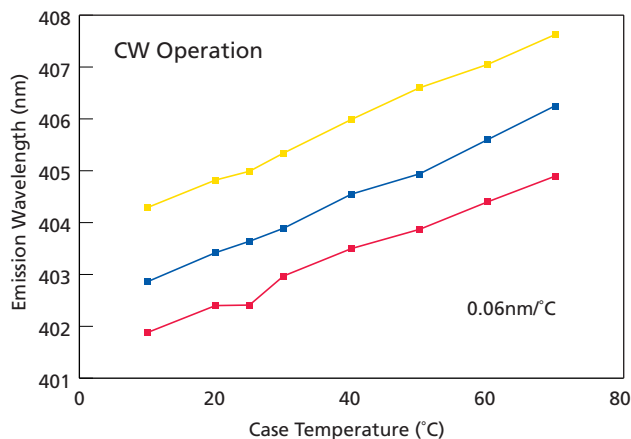


Fig. 11. Temperature dependence of the peak emission wavelength of three LDs under CW operation at an output power of 5 mW.

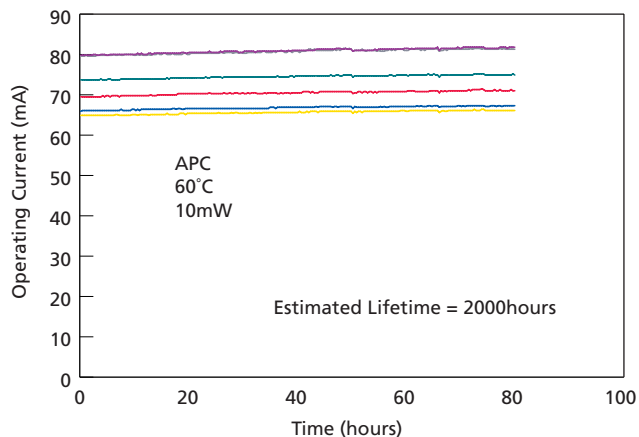


Fig. 12. Operating current of InGaN-MQW/GaN/AlGaIn SCH LDs as a function of time under a constant output power of 5 mW at an ambient temperature of 50°C controlled using an autpower controller.

4. Conclusions

UV InGaN and GaN LEDs were grown on ELOG and sapphire substrates. When the emission wavelength of InGaN LEDs was shorter than 380 nm, EQE of the InGaN LED on ELO was much higher than that on sapphire at high currents. At low currents, both LEDs had the same EQE. When the active layer was GaN, EQE of the LED on sapphire was relatively low, both at low and high currents, due to the lack of localized energy states formed by In composition fluctuations. When the emission wavelength was in the blue and green regions, EQE was almost the same between LEDs on ELOG and sapphire due to a large number of deep localized energy states formed by large In com-

position fluctuations. EQE gradually decreases with decreasing emission wavelength of InGaN LEDs from 470 nm to 370 nm in spite of decreasing the strain in the InGaN well layer. These results cannot be explained by QCSE.

Only the localized energy states formed by In composition fluctuations can explain these results. The operating current of the LD is much higher than that of LEDs. Thus, under the operating conditions of the laser diodes, carriers injected into InGaN well layers easily overflow from the localized energy states, and reach nonradiative recombination centers formed by a large number of TDs. Thus, in order to improve the lifetime of the LD, the TD had to be reduced using ELOG substrate. InGaN-MQW/

GaN/AlGaIn SCH LDs were fabricated on the ELOG. The LDs with cleaved mirror facets showed an output power as high as 40 mW under RT-CW operation with a stable fundamental transverse mode. The lifetime of the LDs at a constant output power of 30 mW was approximately 500 hours under CW operation at an ambient temperature of 60°C. High power LDs with an output power of 30 mW and a lifetime of 3,000 hours will be available soon because rate of progress in improvement of the lifetime is so fast.

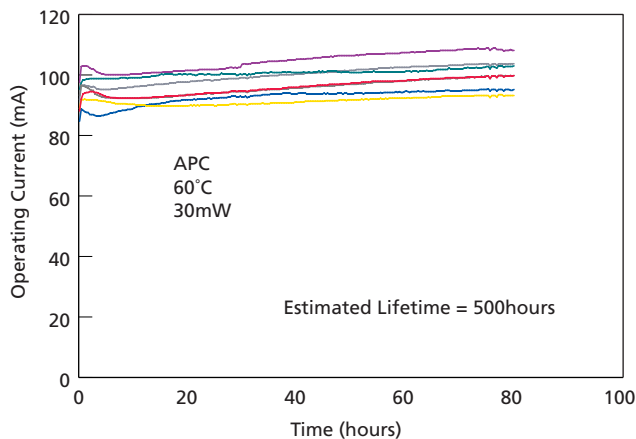


Fig. 13. Operating current of InGaN-MQW/GaN/AlGaIn SCH LDs as a function of time under a constant output power of 30 mW at an ambient temperature of 60°C controlled using an autpower controller.

References

- 1) S. Yoshida, S. Misawa and S. Gonda: Appl. Phys. Lett. **42**, 427 (1983) .
- 2) H. Amano, N. Sawaki, I. Akasaki and T. Toyoda: Appl. Phys. Lett. **48**, 353 (1986) .
- 3) For a review, see S. Nakamura and G. Fasol: The Blue Laser Diode, 1sted. (Springer-Verlag, Heidelberg, 1997) .
- 4) S. Nakamura: Jpn. J. Appl. Phys. **30** , L1705 (1991) .
- 5) S. Strite and H. MorkoÁ, J. Vac. Sci & Technol. B **10**, 1237 (1992).
- 6) F. A. Ponce and D. P. Bour: Nature **386**, 351 (1997) .
- 7) J. I. Pankove, E. A. Miller and J. E. Berkeyheiser: RCA Review **32**, 383 (1971).
- 8) J. I. Pankove, M. T. Duffy, E. A. Miller and J. E. Berkeyheiser: J. Luminescence **8**, 89 (1973) .
- 9) H. P. Maruska, W. C. Rhines and D. A. Stevenson: Mat. Res. Bull. **7**, 777 (1972) .
- 10) O. Lagerstedt and B. Monemar: J. Appl. Phys. **45**, 2266 (1974) .
- 11) H. Amano, M. Kito, K. Hiramatsu and I. Akasaki: Jpn. J. Appl. Phys. **28** , L2112 (1989) .
- 12) S. Nakamura, T. Mukai, M. Senoh and N. Iwasa: Jpn. J. Appl. Phys. **31**, L139 (1992) .
- 13) S. Nakamura, N. Iwasa, M. Senoh and T. Mukai: Jpn. J. Appl. Phys. **31**, 1258 (1992) .
- 14) C. Wang and R. F. Davis: Appl. Phys. Lett. **63**, 990 (1993) .
- 15) M. Rubin, N. Newman, J. S. Chan, T. C. Fu and J. T. Ross: Appl. Phys. Lett. **64**, 64 (1994) .
- 16) M.S.Brandt, N.M.Johnson, R. J. Molnar, R. Singh and T. D. Moustakas: Appl. Phys. Lett. **64**, 2264 (1994) .
- 17) J. M. Zavada, R. G. Wilson, C. R. Abernathy and S. J. Pearton: Appl. Phys. Lett. **64**, 2724 (1994) .
- 18) J. Neugebauer and C. Van De Walle: Phys. Rev. B **50**, 8067 (1994) .
- 19) T. Nagatomo, T. Kuboyama, H. Minamino and O. Omoto: Jpn. J. Appl. Phys. **28**, L1334 (1989) .
- 20) T. Matsuoka, H. Tanaka, T. Sasaki and A. Katsui: Inst. Phys. Conf. Ser. **106**, 141 (1990) .
- 21) T. Matsuoka: J. Cryst. Growth **124**, 433 (1992) .
- 22) S. Nakamura and T. Mukai: Jpn. J. Appl. Phys. **31**, L1457 (1992) .
- 23) S. Nakamura, T. Mukai, M. Senoh, S. Nagahama and N. Iwasa: J. Appl. Phys. **74**, 3911 (1993) .
- 24) S. Chichibu, T. Azuhata, T. Sota and S. Nakamura: Appl. Phys. Lett. **69**, 4188 (1996) .
- 25) S. Chichibu, T. Azuhata, T. Sota and S. Nakamura: Appl. Phys. Lett. **70**, 2822 (1997) .
- 26) Y. Narukawa, Y. Kawakami, Sz. Fujita, Sg. Fujita and S. Nakamura: Phys. Rev. B **55**, 1938 (1997) .
- 27) Y. Narukawa, Y. Kawakami, M. Funato, Sz. Fujita, Sg. Fujita and S. Nakamura: Appl. Phys. Lett. **70**, 981 (1997) .
- 28) S. Chichibu, K. Wada and S. Nakamura: Appl. Phys. Lett. **71**, 2346 (1997) .
- 29) S. Nakamura, T. Mukai and M. Senoh: Appl. Phys. Lett. **64**, 1687 (1994) .
- 30) S. Nakamura, M. Senoh, N. Iwasa, S. Nagahama, T. Yamada and T. Mukai: Jpn. J. Appl. Phys. **34**, L1332 (1995) .
- 31) T. Mukai, D. Morita and S. Nakamura: J. Crystal Growth **189/190**, 778 (1998) .
- 32) T. Mukai, H. Narimatsu and S. Nakamura: Jpn. J. Appl. Phys. **37**, L479 (1998) .
- 33) S. Nakamura, M. Senoh, S. Nagahama, N. Iwasa, T. Yamada, T. Matsushita, H. Kiyoku and Y. Sugimoto: Jpn. J. Appl. Phys. **35**, L74 (1996) .
- 34) K. Itaya, M. Onomura, J. Nishino, L. Sugiura, S. Saito, M. Suzuki, J. Rennie, S. Nunoue, M. Yamamoto, H. Fujimoto, Y. Kokubun, Y. Ohba, G. Hatakoshi and M. Ishikawa: Jpn. J. Appl. Phys. **35**, L1315 (1996) .
- 35) G. E. Bulman, K. Doverspike, S. T. Sheppard, T. W. Weeks, H. S. Kong, H. M. Dieringer, J. A. Edmond, J. D. Brown, J. T. Swindell and J. F. Schetzna: Electron. Lett. **33**, 1556 (1997) .
- 36) M. P. Mack, A. Abare, M. Aizcorbe, P. Kozodoy, S. Keller, U. K. Mishra, L. Coldren, and S. DenBaars, MRS Internet J. Nitride Semicond. Res. **2**, 41 (1997) . (Available from <http://nsr.mij.mrs.org/2/41/>)
- 37) A. Kuramata, K. Domen, R. Soejima, K. Horino, S. Kubota and T. Tanahashi: Jpn. J. Appl. Phys. **36**, L1130 (1997) .
- 38) F. Nakamura, T. Kobayashi, T. Asatsuma, K. Funato, K. Yanashima, S. Hashimoto, K. Naganuma, S. Tomioka, T. Miyajima, E. Morita, H. Kawai and M. Ikeda: J. Cryst. Growth **189/190**, 841 (1998) .
- 39) M. Kneissl, D. P. Bour, N. M. Johnson, L. T. Romano, B. S. Krusor, R. Donaldson, J. Walker and C. D. Dunnrowicz: Appl. Phys. Lett. **72**, 1539 (1998) .
- 40) H. Katoh, T. Takeuchi, C. Anbe, R. Mizumoto, S. Yamaguchi, C. Wetzel, H. Amano, I. Akasaki, Y. Kaneko, and N. Yamada: Jpn. J. Appl. Phys. **37**, L444 (1998) .

-
- 41) S. Nakamura, M. Senoh, S. Nagahama, N. Iwasa, T. Yamada, T. Matsushita, H. Kiyoku, Y. Sugimoto, T. Kozaki, H. Umemoto, M. Sano and K. Chocho: *Appl. Phys. Lett.* **72**, 211 (1998) .
- 42) S. Nakamura, M. Senoh, S. Nagahama, N. Iwasa, T. Yamada, T. Matsushita, H. Kiyoku, Y. Sugimoto, T. Kozaki, H. Umemoto, M. Sano and K. Chocho: *Jpn. J. Appl. Phys.* **36**, L1568 (1997) .
- 43) S. Nakamura, M. Senoh, S. Nagahama, N. Iwasa, T. Yamada, T. Matsushita, H. Kiyoku, Y. Sugimoto, T. Kozaki, H. Umemoto, M. Sano and K. Chocho: *Jpn. J. Appl. Phys.* **37**, L627 (1998) .
- 44) S. Nakamura, M. Senoh, S. Nagahama, N. Iwasa, T. Yamada, T. Matsushita, H. Kiyoku, Y. Sugimoto, T. Kozaki, H. Umemoto, M. Sano and K. Chocho: *Jpn. J. Appl. Phys.* **37**, L309 (1998) .
- 45) S. Nakamura, M. Senoh, S. Nagahama, T. Matsushita, H. Kiyoku, Y. Sugimoto, T. Kozaki, H. Umemoto, M. Sano and T. Mukai: *Jpn. J. Appl. Phys.* **38**, L226 (1999) .
- 46) S. D. Lester, F. A. Ponce, M. G. Craford and D. A. Steigerwald: *Appl. Phys. Lett.* **66**, 1249 (1995) .
- 47) D. Kapolnek, X. H. Wu, B. Heying, S. Keller, B. Keller, U. K. Mishra, S. P. Denbaars and J. S. Speck: *Appl. Phys. Lett.* **67**, 1541 (1995) .
- 48) X. H. Wu, P. Fini, S. Keller, E. J. Tarsa, B. Heying, U. K. Mishra, S. P. DenBaars and J. S. Speck: *Jpn. J. Appl. Phys.* **35**, L1648 (1996).
- 49) B. Heying, X. H. Wu, S. Keller, Y. Li, D. Kapolneck, B. P. Keller, S. P. Denbaars and J. S. Speck: *Appl. Phys. Lett.* **68**, 643 (1996) .
- 50) F. A. Ponce, D. P. Bour, W. Gotz and P. J. Wright: *Appl. Phys. Lett.* **68**, 57 (1996) .
- 51) B. Garni, J. Ma, N. Perkins, J. Liu, T. F. Kuech, and M. G. Lagally: *Appl. Phys. Lett.* **68**, 1380 (1996) .
- 52) S. J. Rosner, E. C. Carr, M. J. Ludowise, G. Girolami and H. I. Erikson: *Appl. Phys. Lett.* **70**, 420 (1997) .
- 53) N. G. Weimann and L. F. Eastman: *J. Appl. Phys.* **83**, 3656(1998).
- 54) P. J. Hansen, Y. E. Strausser, A. N. Erickson, E. J. Tarsa, P. Kozodoy, E. G. Brazel, J. P. Ibbetson, U. Mishra, V. Narayanamurti. P. Denbaars and J. S. Speck: *Appl. Phys. Lett.* **72**, 2247 (1998) .
- 55) W. Qian, G. S. Rohrer, M. Skowronski, K. Doverspike, L. B. Rowland and D. K. Gaskill, *Appl. Phys. Lett.* **67**, 2284 (1995) .
- 56) X. H. Wu, L. M. Brown, D. Kapolnek, S. Keller, B. Keller, S. P. Denbaars and J. S. Speck, *J. Appl. Phys.* **80**, 3228 (1996) .
- 57) E. J. Tarsa, B. Heying, X. H. Wu, P. Fini, S. P. Denbaars and J. S. Speck, *J. Appl. Phys.* **82**, 5472 (1997) .
- 58) T. Sugahara, H. Sato, M. Hao, Y. Naoi, S. Kurai, S. Tottori, K. Yamashita, K. Nishino, L. T. Romano and S. Sakai: *Jpn. J. Appl. Phys.* **37**, L398 (1998) .
- 59) S. Chichibu, H. Marchand, M. S. Minsky, S. Keller, P. T. Fini, J. P. Ibbetson, S. B. Fleischer, J. S. Speck, J. E. Bowers, E. Hu, U. K. Mishra, S. P. DenBaars, T. Deguchi, T. Sota and S. Nakamura: *Appl. Phys. Lett.* **74**, 1460 (1999) .
- 60) M. D. McCluskey, C. G. Van de Walle, C. P. Master, L. T. Romano and N. M. Johnson, *Appl. Phys. Lett.* **72**, 2725 (1998) .
- 61) H. Sato, T. Sugahara, Y. Naoi and S. Sakai: *Jpn. J. Appl. Phys.* **37**, 2013 (1998) .
- 62) S. Keller, U. K. Mishra, S. P. Denbaars and W. Seifert, *Jpn. J. Appl. Phys.* **37**, L431 (1998) .
- 63) A. Usui, H. Sunakawa, A. Sakai and A. Yamaguchi: *Jpn. J. Appl. Phys.* **36**, L899 (1997) .
- 64) O. H. Nam, M. D. Bremser, T. Zheleva and R. F. Davis: *Appl. Phys. Lett.* **71**, 2638 (1997) .
- 65) T. Mukai, K. Takekawa and S. Nakamura: *Jpn. J. Appl. Phys.* **37**, L839 (1998) .
- 66) T. Mukai, M. Yamada and S. Nakamura: *Jpn. J. Appl. Phys.* **37**, L1358 (1998) .
- 67) S. Nakamura: *Science* **281**, 956 (1998) .
- 68) T. Takeuchi, S. Sota, M. Katsuragawa, M. Komori, H. Takeuchi, H. Amano and I. Akasaki: *Jpn. J. Appl. Phys.* **36**, L382 (1997) .
- 69) D. L. Smith and C. Mailhot: *Phys. Rev. Lett.* **58**, 1264 (1987) .
- 70) M. B. Nardelli, K. Rapcewicz and J. Bernholc: *Appl. Phys. Lett.* **71**, 3135 (1997) .
- 71) J. S. Im, H. Kollmer, J. Off, A. Sohmer, F. Scholz and A. Hangleiter: *Phys. Rev. B* **57**, R9435 (1998) .
- 72) I. Ho and G. B. Stringfellow: *Appl. Phys. Lett.* **69**, 2701 (1996) .
- 73) S. Nakamura, M. Senoh, S. Nagahama, N. Iwasa, T. Yamada, T. Matsushita, Y. Sugimoto and H. Kiyoku: *Appl. Phys. Lett.* **70**, 868 (1997) .
- 74) S. Nakamura, M. Senoh, S. Nagahama, N. Iwasa, T. Yamada, T. Matsushita, Y. Sugimoto, and H. Kiyoku: *Appl. Phys. Lett.* **70**, 1417 (1997) .
- 75) S. Nakamura, M. Senoh, S. Nagahama, N. Iwasa, T. Yamada, T. Matsushita, H. Kiyoku, Y. Sugimoto, T. Kozaki, H. Umemoto, M. Sano and K. Chocho: *Jpn. J. Appl. Phys.* **37**, L1020 (1998) .